THE ASTROPHYSICAL JOURNAL, 510:474–484, 1999 January 1

BRIGHT POINTS AND SUBFLARES IN ULTRAVIOLET LINES AND X-RAYS

M. ROVIRA,[1] B. SCHMIEDER,[2,3] P. DÉMOULIN,[2] G. M. SIMNETT,[4] M. J. HAGYARD,[5]
E. REICHMANN,[5] AND E. TANDBERG-HANSSEN[5]
Received 1998 April 9; accepted 1998 April 14

ABSTRACT

We have analyzed an active region which was observed in Hα (Multichannel Subtractive Double Pass Spectrograph), in UV lines (*SMM*/UVSP), and in X-rays (*SMM*/HXIS). In this active region there were only a few subflares and many small bright points visible in UV and in X-rays. Using an extrapolation based on the Fourier transform, we have computed magnetic field lines connecting different photospheric magnetic polarities from ground-based magnetograms. Along the magnetic inversion lines we find two different zones: (1) a high-shear region ($>70°$) where subflares occur, and (2) a low-shear region along the magnetic inversion line where UV bright points are observed. In these latter regions the magnetic topology is complex with a mixture of polarities. According to the velocity field observed in the Si IV λ1402 line and the extrapolation of the magnetic field, we notice that each UV bright point is consistent with emission from low-rising loops with downflows at both ends. We notice some hard X-ray emissions above the bright-point regions with temperatures up to 8×10^6 K, which suggests some induced reconnection due to continuous emergence of new flux. This reconnection is also enhanced by neighboring subflares.

Subject headings: Sun: flares — Sun: UV radiation — Sun: X-rays, gamma rays

1. INTRODUCTION

Active Region (AR) 2725 (Hale region 17188) crossed the central meridian on 1980 October 13. It was the return of Hale regions 17120 and 17127, and by October 13 it had increased its Ca II plage area from about 4000 millionths of the solar disk to about 8000 millionths since the previous central meridian crossing. Similarly, the region's sunspot area had tripled. The region was magnetically complex of the type $\alpha\beta\gamma$. Consequently, one would expect it to be a candidate for considerable flare activity. Large flares occur mainly in compact regions when energy can be built up over the previous hours or days. In a complex topology many small events occur which favor a quasi-continuous release of energy (Amari et al. 1997).

On October 12 the region produced small, impulsive flare brightenings preceding an SB flare at 02:00 UT, observed both in UV lines and in hard X-rays (Tandberg-Hanssen, Reichmann, & Woodgate 1983). The region was also studied on October 14 when a 3B flare occurred around 0600 UT, again producing both UV lines and hard X-rays (Cheng et al. 1981).

In the present paper we analyzed data from the active region on October 13, a day when AR 2725 did not exhibit any particularly important solar activity, but rather a number of small events that testify basically to a very active period, with magnetic flux emergence, prominence activation, two-ribbon flare activity, and bright-point oscillations.

We shall discuss these manifestations in a framework where we give information on the temperature and density of the plasma, and on the development of the magnetic field in the active region. We further analyze the plasma motions in the flare regions, in the prominences, as well as in several bright points visible in UV, X-rays, and Hα. The overall picture that will emerge is of a very active region where the development of the magnetic field leads to a continuous miniflaring activity due to the copious energy releases. We find that the UV-bright points occur along magnetic inversion lines.

[1] Instituto de Astronomia y Fisica del Espacio, IAFE-CONICET, CC.67, Suc.28, 1428, Buenos Aires, Argentina.
[2] Observatoire de Paris, Section Meudon, URA2080, DASOP, 92195, Meudon Cedex Principal, France.
[3] Institute of Theoretical Astrophysics, Blindern, N0315, Oslo, Norway.
[4] University of Birmingham, Edgbaston, Birmingham, B152TT, England, UK.
[5] NASA Marshall Space Flight Center, Huntsville, AL 35812.

2. OVERVIEW OF THE DATA

2.1. Hα

The Multichannel Subtractive Double Pass (MSDP) instrument (Mein 1977) was observing at the Meduon Solar Tower during the flare at 09:48 UT on 1980 October 13. This instrument provides nine channels through the Hα line profile, and we can reconstruct the profiles of the line with nine points observed simultaneously over a given region, whence maps of intensity and Doppler shifts are derived (Fig. 1). We use the map obtained in the near continuum of Hα to identify the sunspots of S1, S2, S3 (Fig. 1*d*), and for overlays with UVSP observations. We notice clearly the two ribbons of the flare (R1 and R2 in Fig. 1*a*) and the postflare loops between them. The ribbon R2 is located over a region of strong magnetic field, and this may be the reason why it appears weaker than the R1. Li et al. (1997) have shown already a similar case and explain it as follows: "Electrons, which they assumed to be the dominant energy carriers, are focused in a small core over the high magnetic area and cannot reach the chromosphere. They are reflected towards the other footpoint which is in a region of lower magnetic strength where heating is then possible at the chromospheric level." While there is no reason to favor electrons over ions in this regard, it does indicate that there is a preferred region of energy deposition at the top of the transition region.

Close to a region of parasitic polarity labeled "P" in Fig. 1*c*, we identify a filament F1 (noted in Fig. 1*a*). The Hα velocity field (Fig. 1*b*) of the filament F1 shows that we have downflows at both ends of F1 and upflows between. This filament F1 has a classical motion of what we call Arch

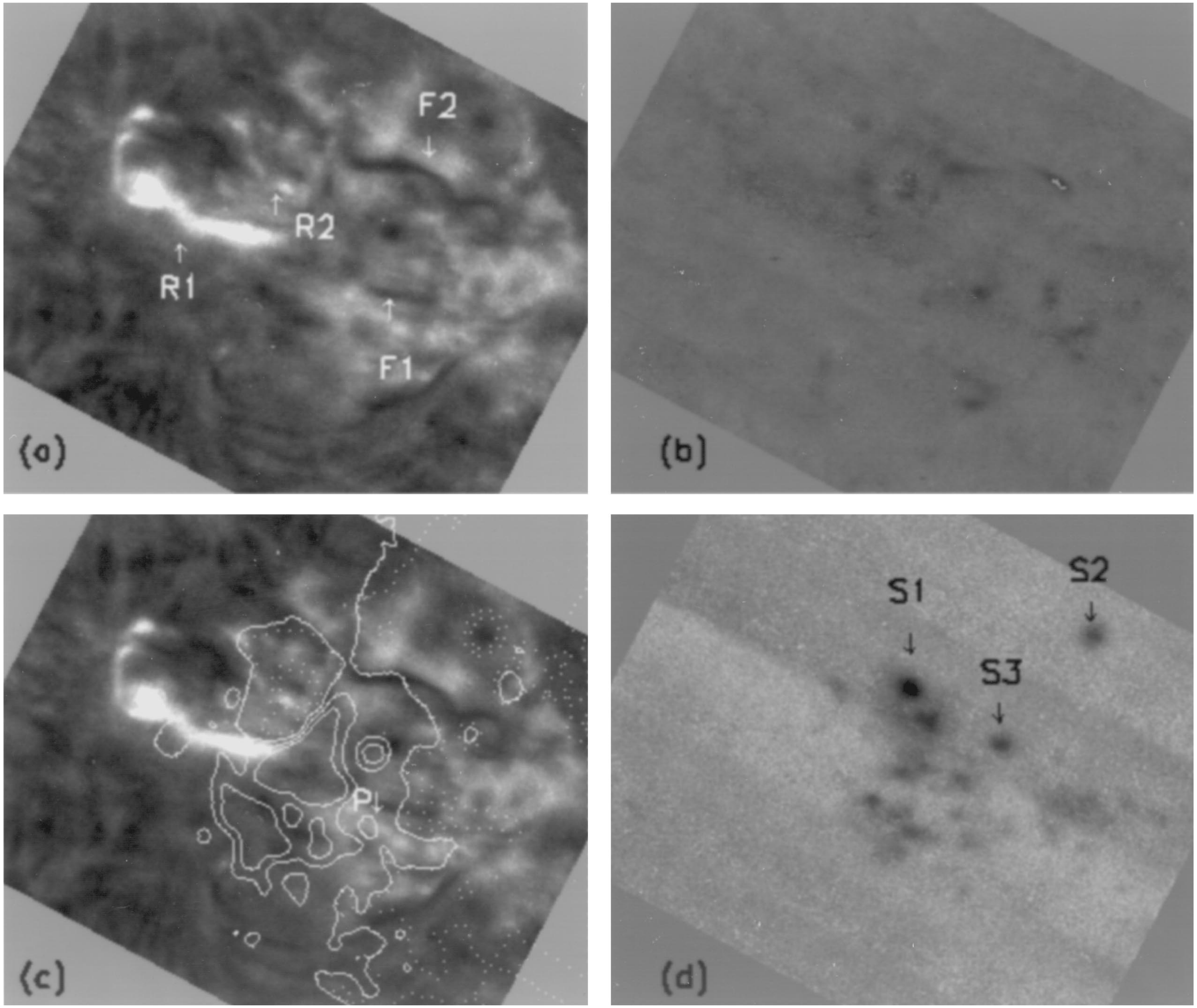

FIG. 1.—AR 2725 observed by the MSDP on 1980 October 13 at 09:48 UT. (*a*) Intensity in Hα line (note the two ribbons of the flare R1 and R2 and two filaments F1 and F2), (*b*) Doppler shift in Hα line (note the twisted motion of the filament F2 and downflows at both ends of F1); (*c*) intensity in Hα line and contour of the magnetic field with arrow pointing to a parasitic polarity P indicated by an arrow below S3; (*d*) intensity in the continuum near Hα (note the sunspots S1, S2, S3).

Filament System (AFS) (Alissandrakis, Tsiropoula, & Mein; Schmieder, Raacht, & Wiik 1991; Mein et al. 1996): the tubes are rising up, while plasma is falling along both ends.

Between the two sunspots S1 and S3 we can detect a filament F2 moving with high velocity in the Doppler shift map (Fig. 1*b*).

2.2. *Ultraviolet*

The ultraviolet spectrometer and polarimeter (UVSP) on the *Solar Maximum Mission* (*SMM*) (Woodgate et al. 1980) was in the rastering mode (80 × 80 pixels of 3 arcsec^2) on 1980 October 13 at 07:34 UT. It was observing in the two lines C IV λ1548 and Si II λ1533 during the first of four orbits we discuss. The resulting data in Si II allow us to identify the sunspots S1, S2, and S3 of region AR 2725 (see Fig. 2*a*). Later during the second, third, and fourth orbits the UVSP observed the same region in the Dopplergram mode at 09:06 UT, 10:42 UT, and 12:18 UT, using the Si IV λ1402 line. Before making a large raster, a spectrum in the wavelength range was obtained. Finally, the large rasters were followed by 20 × 20 pixel rasters, centered on different small brightenings named, e.g., B, C, D, and E (Fig. 2). We use Figures 2*c* and 2*d* to define the locations, in this active region complex, where bright points were observed during one orbit of the day of 1980 October 13. Location B, composed of three individual pixels orientated north-south, and C, extended east-west, are the location of the bright points

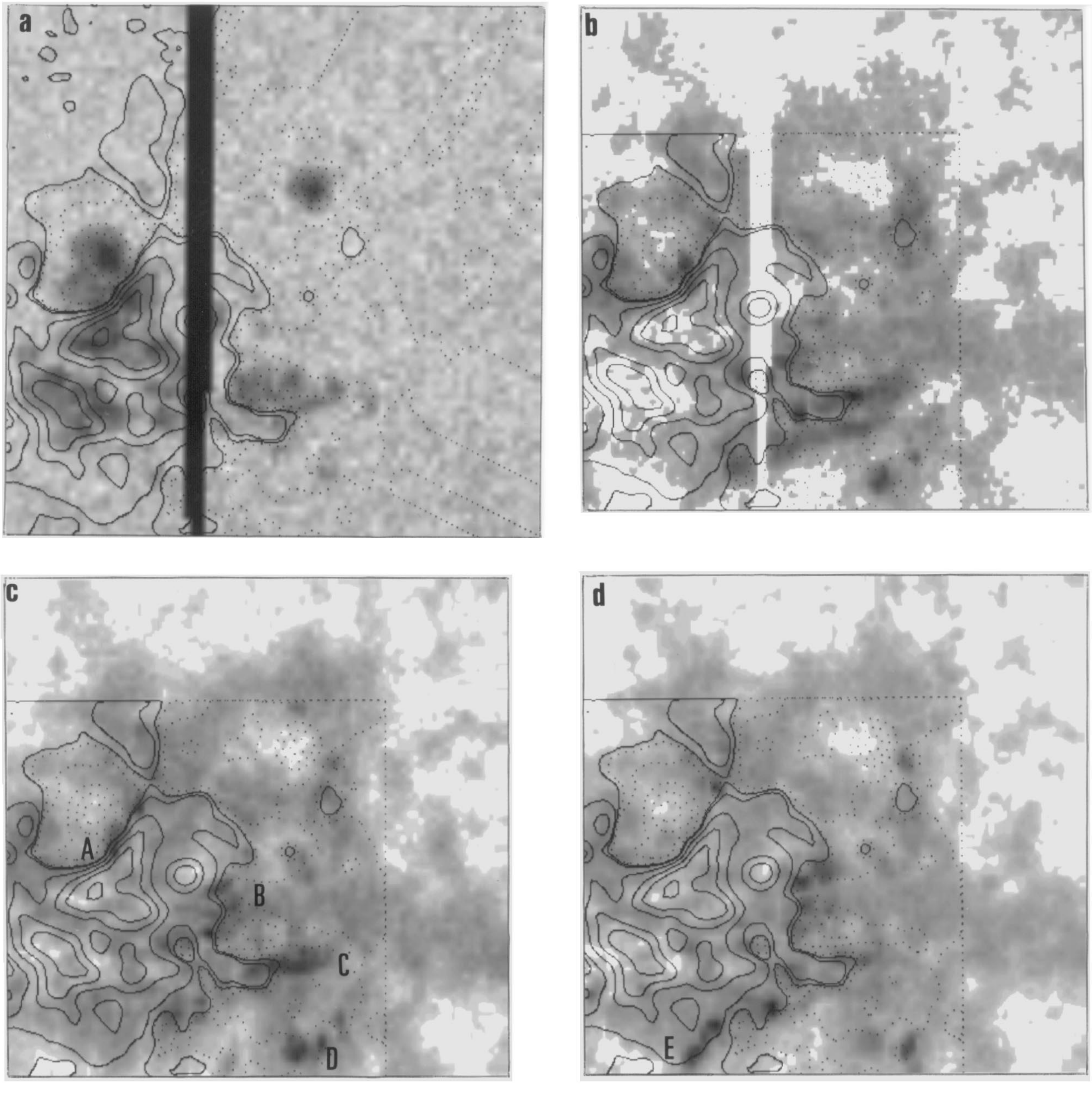

FIG. 2.—AR 2725 observed on 1980 October 13, by the UVSP (*a*) in the Si II line and (*b*) in the C IV line at 07:34 UT, and (*c*) in Si IV at 09:06 UT and (*d*) at 10:42 UT. Bright points A, B, C, D, E (dark regions according to the color table) are labeled.

that appeared successively in the second orbit, while locations D and E are those of the bright points appearing after 10:42 UT and which were observed to have intermittent brightness fluctuations (see § 3). Location A is the region of the brightening, corresponding to the location of the flares on the eastern edge of the region, missed by UVSP, but observed by HXIS (§ 2.4) and in Hα on the ground (see above).

Several bright points in the active region complex were observed in the small raster mode of UVSP, using the Si IV line. By studying successive raster maps, one clearly discerns brightness fluctuations of a quasi-periodic nature in several of the bright points. During the second orbit bright point B is active at 09:06 UT (mean time of the large raster) and between 09:25 and 09:50 UT with two enhancements (Fig. 3*a*). A particularly well-observed case in the fourth orbit is shown in Figure 3*b* where two adjacent pixels (2000″ × 2000″ each) increase and fade in brightness out of phase with each other. The lifetime of each bright pixel is less than 20 minutes. This might indicate successive reconnections in adjacent locations (§ 3.2.1).

In the Si IV Dopplergrams (Fig. 4) over the bright loops we identify blueshift along the magnetic inversion line and redshifts on both sides. These results are consistent with those of Klimchuk (1987), who finds a marked preference for blueshifts in magnetic corridors and redshifts in strong field regions (except above sunspots).

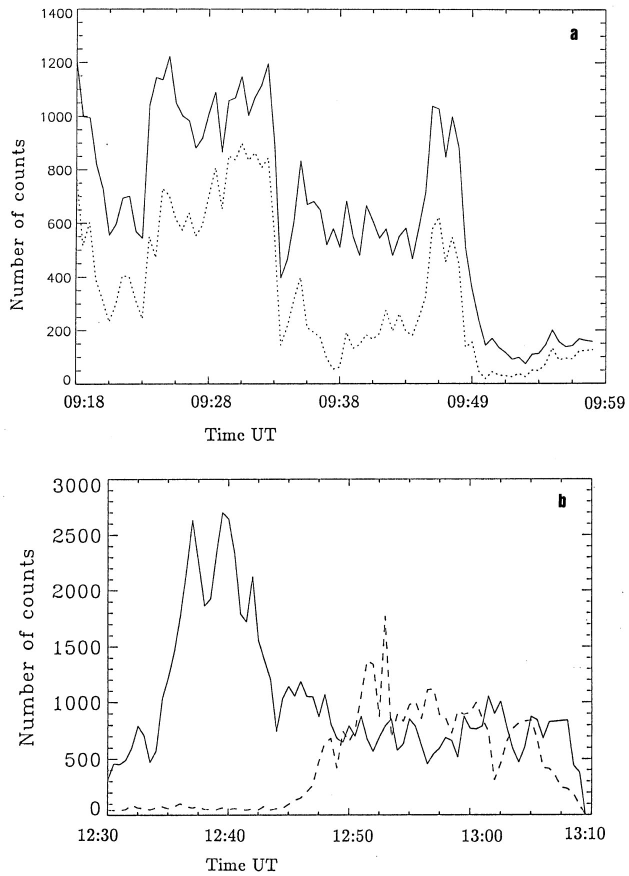

FIG. 3.—Light curves of Si IV bright points (pixel = 3 × 3 arcsec^2). (*a*) Bright point B observed during the second orbit. Solid line represents the sum of the emission of all the B area; dotted line, the emission of the brightest pixel. (*b*) Two individual and adjacent pixels during the fourth orbit. The lifetime of a bright point is less than 20 minutes with plateau and peak of shorter durations.

2.3. *Magnetic Field*

Marshall Space Flight Center (MSFC) obtained a number of vector magnetograms during the October 12–14 period, of which four are available for October 13, viz. at 14:26, 15:23, 18:09, and 20:52 UT. We have identified three sunspots: S1 (negative polarity enclosed in a positive polarity), S2 (preceding negative polarity), and S3 (positive polarity), plus a region of parasitic polarity, P (below S3 Figs. 1*c* and *d*) on the magnetic field map. These data allow us to follow the evolution of the parasitic polarity, P (see Fig. 5). On October 12 the negative polarity shows a protruding area that evolves to form an isolated "island" on the following day at 14:26 UT. Unfortunately, we have no magnetic field data for times in between which correspond to the time of the subflare we are studying. The magnetic shear is computed from the transverse field by the method developed by Teuber, Tandberg-Hanssen, & Hagyard (1977). The magnetic shear angle is the difference between the directions of the observed and the potential transverse fields. We note that strong shear ($>70°$) is present only in the vicinity of the sunspot (S1) (Fig. 5, *lower right*).

We perform the magnetic field extrapolation by using the magnetogram obtained at 15:06 UT and provided by Kitt Peak National Observatory because we need a large field of view around the active region in order to have a balance of the positive and negative magnetic field flux. We used the method of Fourier transform developed first by Alissandrakis (1981) and later by Démoulin et al. (1997) The extrapolation results, both in a potential and in a linear force-free field configuration, are shown in Figure 6 and can be summarized as follows:

1. In regions B and C of the UV bright points potential linkage lines between positive and negative polarities (Fig. 6*c*) may explain the small loops visible in UV (bright points).

2. In the region of subflares we have to introduce a shear $\nabla \times \boldsymbol{B} = \alpha \boldsymbol{B}$ ($\alpha = -1.9 \times 10^{-2}$ Mm^{-1}), where α is constant, in the configuration in order to account for the Hα-bright ribbons visible at 09:48 UT. Apparently the postflare loops visible in Hα follow well the extrapolated lines shown in Figure 6*d*.

2.4. *HXIS*

The HXIS observations cover a coarse field of view of 6′24″ × 6′24″ with a resolution of 32″, within which there is a central region of fine field of view where the resolution is 8″. The X-ray intensity of all pixels is acquired simultaneously in six energy bands from 3.5 to 30 keV, of which only the lower four energy bands are useful for the present analysis. HXIS has two modes: a flare mode where the time resolution is 3.0 s, and a quiet mode where the time resolution is 15.4 s. We have used data mainly from the 3.5–5.5 and 5.5–8.0 keV channels since the others have relatively few counts during the modest flare activity we are discussing. Figure 7 shows how the HXIS and UVSP fields of view overlap.

The analysis of HXIS for the three orbits beginning at 07:09 UT, 08:44 UT, and 10:19 UT shows two subflares occurring, respectively, at 07:23 UT and at 09:45 UT, at the location (region e) corresponding to the Hα 2 ribbons and another source of emission (region d) overlying roughly the region (B–C) corresponding to the UV bright points in Figure 7. The shape of these two sources changes slightly

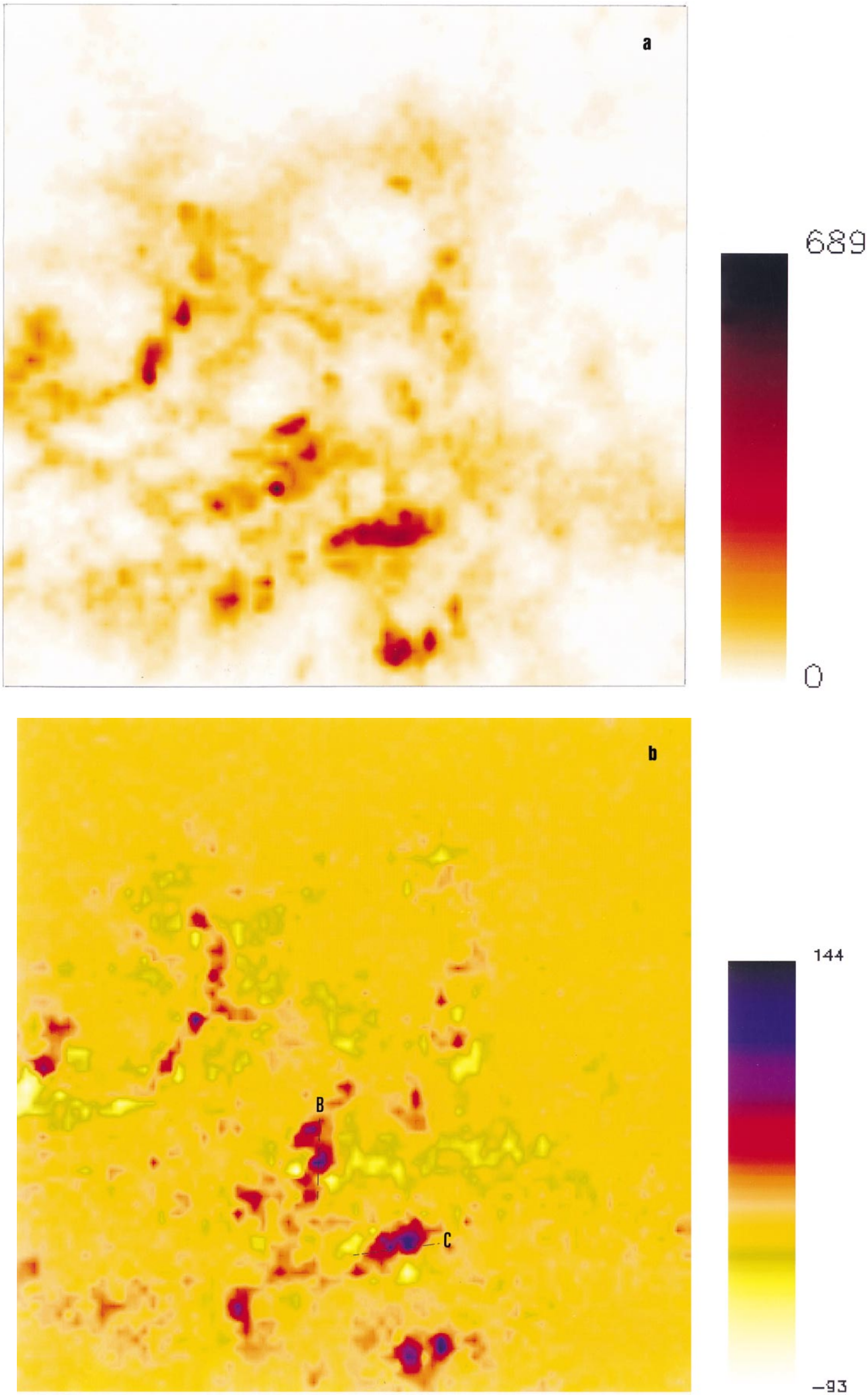

FIG. 4.—(*a*) Intensity map and (*b*) dopplergram in the Si IV line at 09:06 UT on 1980 October 13 observed with the UVSP spectrometer aboard the solar mission *SMM*. B and C are UV bright points. In (*b*) blue is blueshift, yellow is redshift; the numbers on the color bar indicate velocities in kilometers, per second, and the dashed lines the local magnetic inversion line.

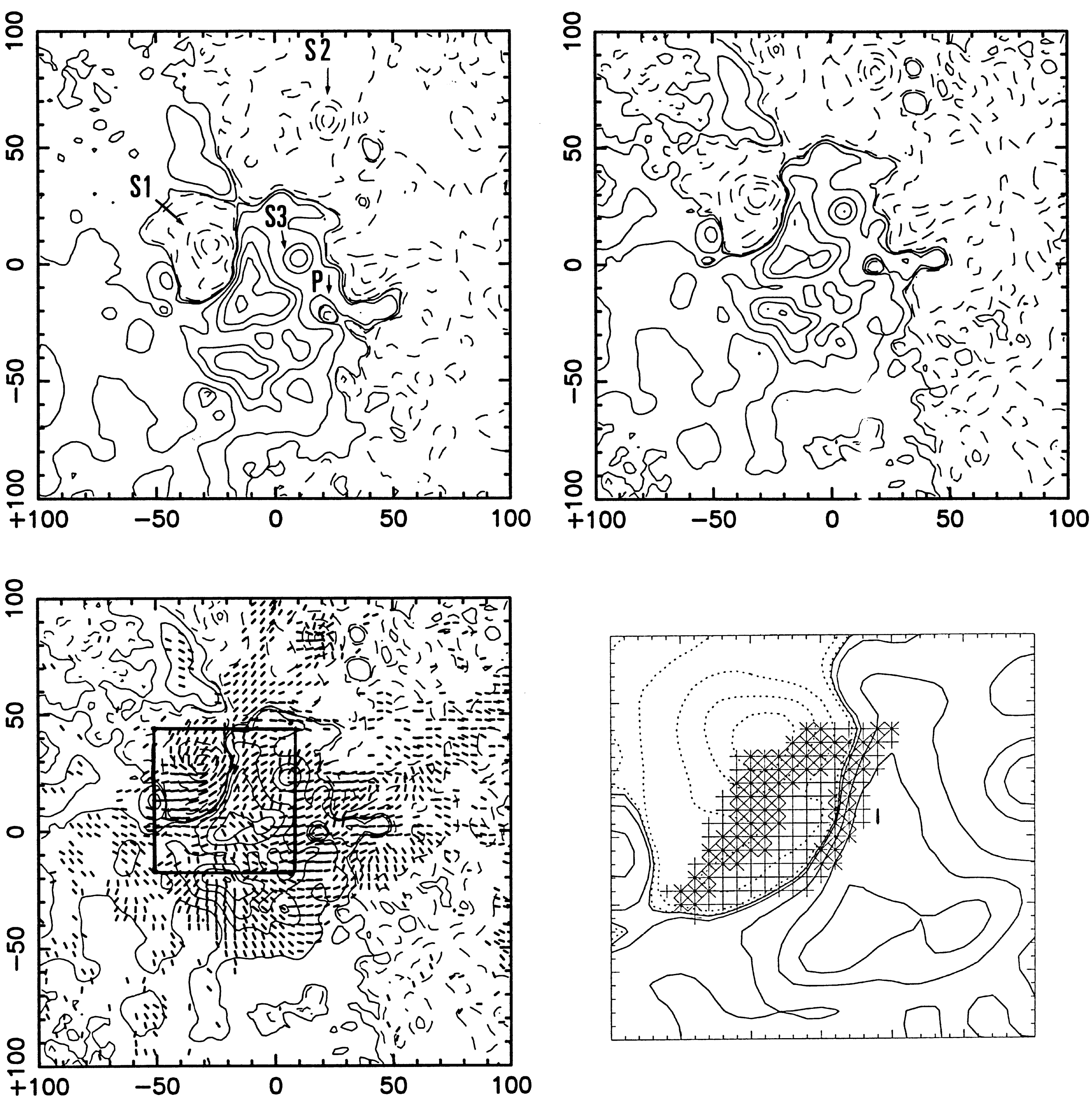

FIG. 5.—Magnetic field maps of AR 2725 from MSFC, longitudinal field on October 13 (*a*) at 14:26 UT, (*b*) at 18:09 UT, (*c*) the observed transverse magnetic field at 18:09 UT, (*d*) longitudinal field at 18:09 UT (partial frame indicated by a box in *c*. Crosses indicate shear angle between 70° and 80°, and the asterisk denotes a shear larger than 80°. The distances are in megameters. The contours are 10, 100, 200, 1000, 1500, and 2000 G.

with time but is virtually constant in the coarse field of view. During the first subflare, bursts coming from both these regions (e and d) are almost in phase. We see an enhancement of the region d emission slightly later (4 minutes) than the emission of region e where a subflare occurs at 07:23 UT (Fig. 8). The distance between regions e and d is $\sim 1.5 \times 10^5$ km; the velocity should be larger than 500 km s^{-1}. If the events are causally related we can envision a thermal front, a particle beam, or an MHD Alfvén wave which transmits the perturbation. A conduction front or a particle beam suggests that a loop does exist between regions e and d. According to the extrapolated magnetic field, no such magnetic field lines are present between these two sites (Fig. 6). This would then tend to favor MHD waves as the transmitting mechanism.

During the second orbit bright-point "precursors" to the second flare occur in regions c (09:10, 09:15 UT) and d (09:05–09:16, 09:25–09:40 UT) which are not directly related to the subflare in region e (09:45 UT) (Fig. 9). The 8″ resolution fine field of view has some resolved parts (a and b) of the flare region visible (region e) within the contours of the coarse field of view (Fig. 7). They correspond to the footpoints of the flaring loop at the onset of the flare. They are well coaligned with the Ha ribbons. Previous observations with HXIS and the *Yohkoh* HXT telescope have shown that footpoint brightenings are commonly observed

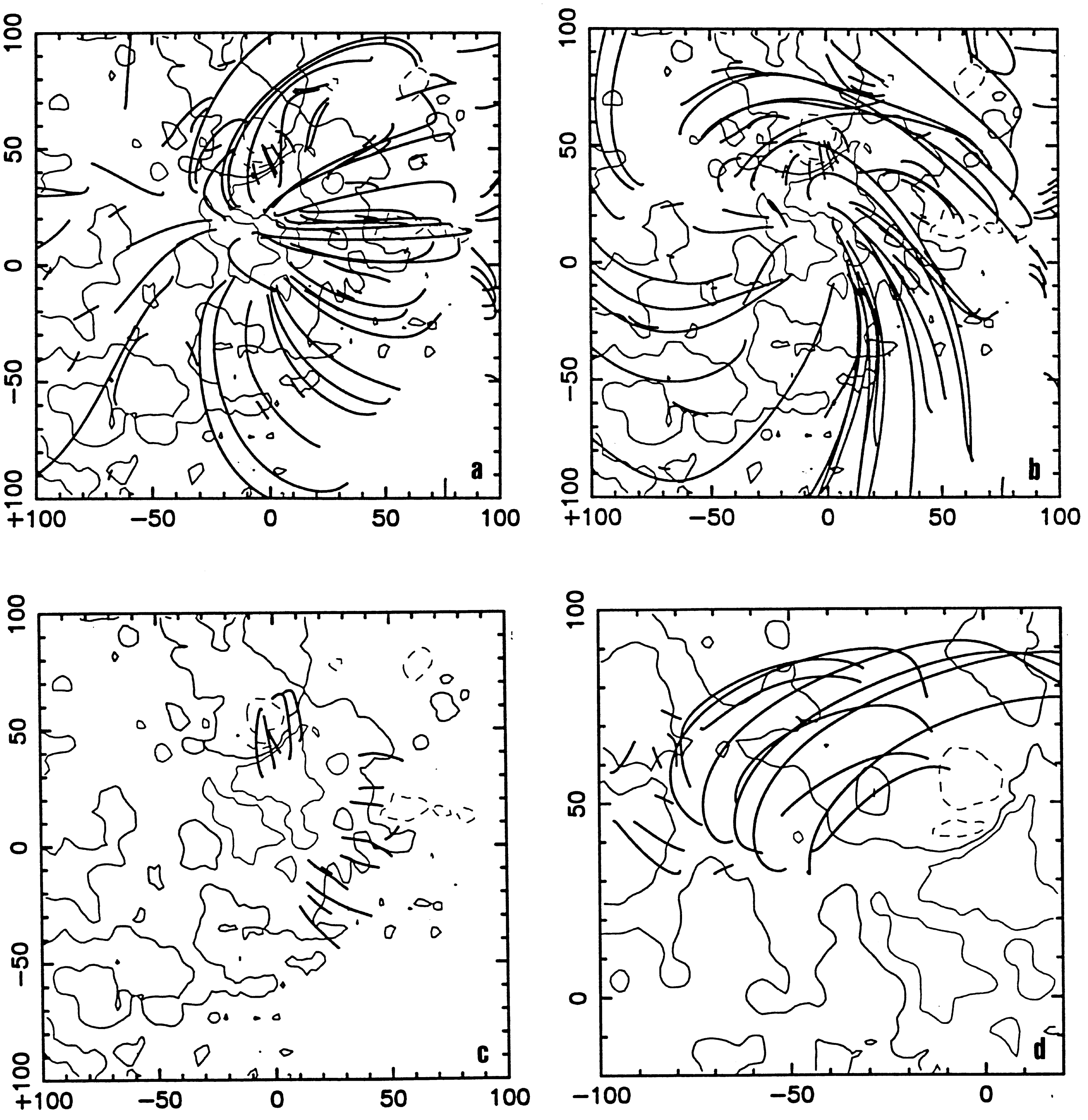

FIG. 6.—Computed extrapolated magnetic field lines from the Kitt Peak magnetic field: (*a*) and (*c*) potential configuration, where in (*c*) only the short field lines have been drawn; (*b*) and (*d*) force free-field configurations; (*d*) a blowup of the flare region, where the field lines correspond well to the postflare loops visible in Fig. 1a, and their feet would be anchored in the bright ribbons R1 and R2. Levels of the contours are 10, 100, 500, 1000, 1500, and 2000 G.

before loop-top brightening (Simnett & Strong 1984), Simnett 1983; Sakao et al. 1998). That from the northerly point in region a had X-ray emission in the 11.5–16 keV energy band which lasted for around 60 s (FWHM). This was the only site of significant X-ray emission at this energy within the HXIS field of view. The hard X-ray burst spectrometer on *SMM* recorded a burst extending to 100 keV, which had a maximum at 09:43:51 UT, 1 minute earlier than the burst seen by HXIS. There was a microwave burst (Solar Geophysical Data, No. 436, Part 1) recorded at 8.4 GHz which started at 09:38 UT and reached a maximum at 09:48 UT. It is likely that the site of this emission was outside the HXIS field of view. A Type III burst was reported at 09:53 UT. Thus, this event not only produced energetic electrons in the corona during the decay, but it showed that there were magnetic field lines also reaching from the flare site to the high corona.

Coming back to the discussion of region d, we identify clearly two bursts with duration of 10 minutes during the second orbit; they are spatially and temporally related to the UV bright points in B. The first burst corresponds to the active period (09:25–09:35 UT). The maximum peak in

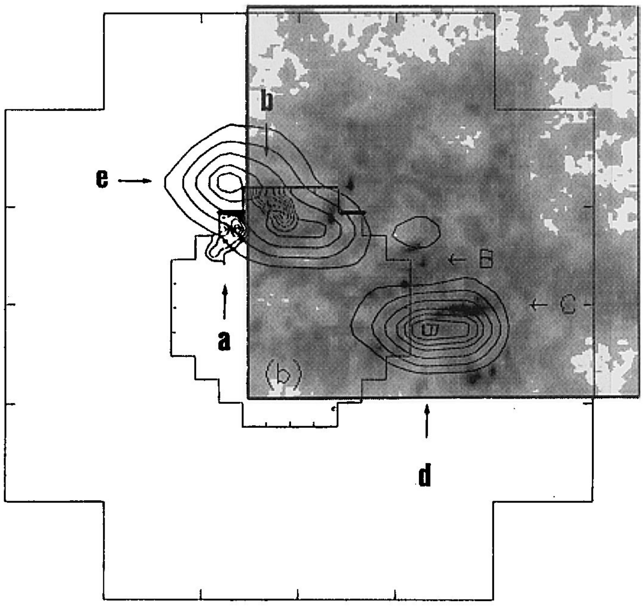

FIG. 7.—UVSP map obtained at 09:06 UT (B and C bright points are indicated) co-aligned with HXIS maps, coarse (contours of the sources e and d between 09:29:20 UT and 09:44:39 UT) and fine fields of view (contours of sources a and b between 09:49:42 UT during the flare time).

X-ray seems to be delayed compared to UV (Figs. 3*a* and Fig. 9). The other UV peak at 09:45 UT corresponds to the flare time observed in region; B would react to far–X-ray emission. We conclude that a certain relationship does exist between these UV and X-ray emissions.

Some plasma parameters for the events on 1980 October 13 have been calculated for three periods: two for region e, and one for region d. The results are shown In Table 1. We were able to get a good two-temperature fit for the flare plasma during the main and the decay phases and a rather good single-temperature fit for the region d. For the temperature fits we have used the HXIS Counting Rate Prediction Programme, which for a given temperature and emission measure predicts the instrument counting rate in each of the six energy bands; the prediction is based on the work of Mewe & Gronenschild (1981). When there are significant counts in the first four HXIS energy bands it is possible to invert the problem to find two temperatures and emission measures which provide the best fit of the data. If there are only significant counts in the lowest two bands then only one temperature and emission measure is possible, and this would not necessarily be consistent with a statistically–insignificant count in the third energy band. Thus a " good " single-temperature fit is one where the prediction produces the observed count in the third energy band.

This is fairly consistent with what we have seen with HXIS in other flares, namely the emission measure increases just after the maximum of the temperature (Schmieder et al. 1996). This occurs both for the high- and low-temperature components. Of course, the two-temperature approximation is just that, and in practice there will be obviously some temperature distribution.

3. ANALYSIS OF THE DATA

The active region AR 2725 on October 13 shows relatively low activity but spasmodic energy releases in different places. The interest of this study is the existence of a large sample of multiwavelength data which gives information on the plasma at different temperatures as well as on the magnetic structures. In order to investigate properly flares and bright points we have important tools to yield the following information: the extrapolation of the magnetic field above the active regions; the knowledge of the velocity field at two different levels in the atmosphere (chromosphere and transition zone); and the high-energy plasma emission.

According to these data we can classify the events occurring in this active region in two classes: (1) the events occurring in the high-shear magnetic region: flare and filaments; and (2) the events appearing in the low-shear magnetic region: arch filament system and UV bright points.

3.1. *Flare and Filament Region*

We have found a strong shear larger than 70° along the inversion line in region A from the transverse magnetic field observed at Marshall Space Flight Center. This is confirmed by the extrapolation study assuming a force-free magnetic field approximation. In that region a subflare occurs, well observed in Hα (double-ribbon flare) and in X-rays. We see plasma with temperatures (10–24] $\times$ 10^6 K) indicating a rapid and intense energy deposition, and we also see evidence of electrons up to 100 keV. The observation of a hard X-ray and microwave burst confirms this. The flare extends toward the east with a long Hα ribbon (R1 in Fig. 1*a*) and an X-ray source also extended in the east-west direction (UVSP was closed at that time).

On the western side of the region of high shear (A) along the inversion line lies the filament F2 (between sunspots S1–S2/S3). During the time of the flare we observe twisting motions along the filament (Fig. 1*b*), suggesting again strong shear of the magnetic field lines.

TABLE 1

TEMPERATURES AND EMISSION MEASURES DURING THE SECOND ORBIT FROM HXIS DATA

Time (UT)	Temperature (K)	EM 1 (cm^{-3})	Temperature 2 (K)	EM 2 (cm^{-3})
		Region e (subflare)		
09:44–09:49......	10.5×10^6	3.2×10^{47}	24×10^6	2.6×10^{45}
09:50–09:52......	9.4×10^6	4.6×10^{47}	20×10^6	7.9×10^{45}
		Region d		
09:31–09:37......	8.4×10^6	4.8×10^{46}		

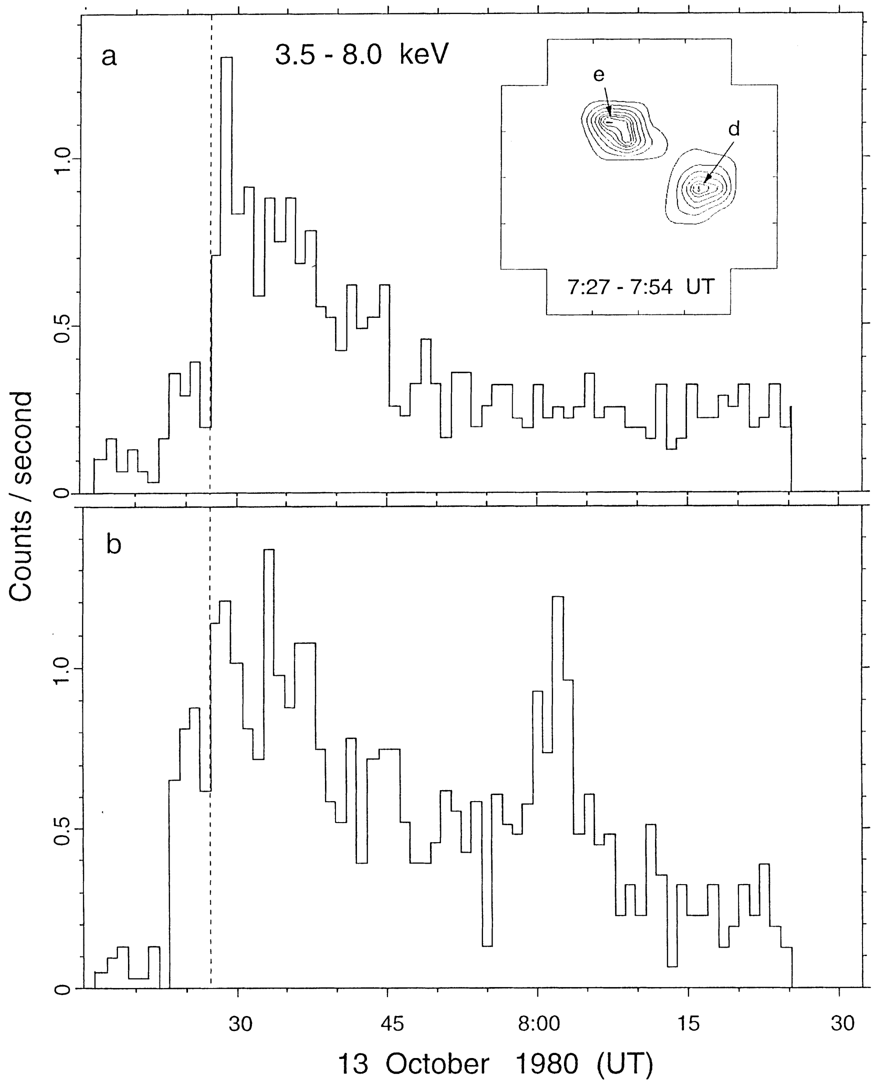

FIG. 8.—HXIS 3.5–8.0 keV X-ray time variation in two resolved regions d and e. Inset is the coarse field-of-view image from 07:27–07:54 UT. Dashed line is drawn to aid the eye at the main onset of the weak event from region d.

3.2. *Arch Filament System and the X-Ray and UV Bright Points*

3.2.1. *Magnetic Configuration*

Let us concentrate now on the southern part of the active region (Fig. 1 and regions B and C in Fig. 2). The inversion line is more or less north-south with some incursions of parasitic polarity (island polarity P and the long tongue of positive polarity). In the latter region we distinguish in Hα the filament F1 (Fig. 1*a*) which is oriented east-west. The extrapolation of the magnetic field (Fig. 6*c*) and the transverse magnetic field (Fig. 5, *lower right*) both indicate low shear in that region. The configuration seems nearly potential, and the field lines are oriented east-west (Fig. 5), *lower right*). The filament F1 has been identified as an arch filament system with downflows at both end and upflows between (§ 2.1 and Fig. 1*b*).

In this region we observe in UV lines bright points that we call B and C overlying the inversion line (Fig. 2). Looking at the velocity field (Fig. 4), we notice upflows in the middle and downflows on both sides of the inversion line. We conclude that these UV bright points are small loops corresponding to the AFS. Because of emerging flux the magnetic field lines are rising from below, transporting to higher levels dense material which falls along the legs of the tubes.

Above the region d, corresponding roughly to regions B–C, low-level hard-X-rays are observed both continuously and sporadically, which suggests some forced or induced reconnection between the emerging field lines and the preexisting coronal lines. Such a mechanism has already been proposed to explain the bright loops observed with *Yohkoh* SXT (10^6 K) above AFS observed in Hα with the multichannel subtractive double pass spectrograph on the German VTT at Tenerife (Malherbe et al. 1998). In the latter paper Malherbe remarks that even the AFS are in a global potential configuration. However, each filament observed with high spatial resolution (0$''$.5) can be fitted only by a magnetic field with an α-value different from zero, providing indications that electric currents are present. Here we have denser plasma at 10^5 (see § 3.2.2) and 8×10^6 K. Apparently the phenomenon of bright loops above AFS exists over a large temperature range.

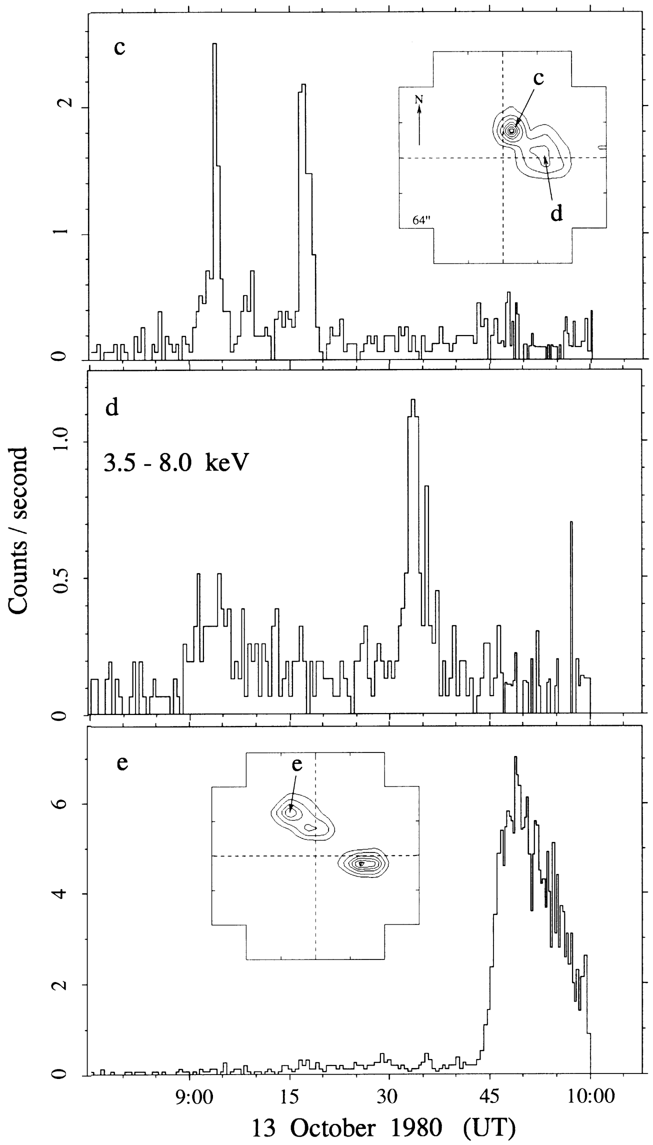

FIG. 9.—HXIS 3.5–8.0 keV time variation of points c, d, and e as defined in Fig. 7. Inset in c is the coarse field of view from 08:58:20 to 09:10:00 UT; and in e from 09:29:20 to 09:44:39 UT.

3.2.2. *Physical Parameters of the UV Plasma of the Bright Points*

We have evaluated the energy using UVSP data as we did previously for a surge and subflare event (Schmieder et al. 1996). Considering the number of counts for the brightest pixels in region B (second orbit), we can calculate the Si IV intensity.

TABLE 2

EMISSION MEASURES DERIVED FROM THE Si IV INTENSITY MEASUREMENTS IN TWO PIXELS IN REGION B OF UV BRIGHT POINTS IN THE SECOND ORBIT (~09:38 UT)

Pixel	Intensity (10^5 ergs cm^{-2} s^{-1})	SEM (10^{27} cm^{-5})	EM (10^{44} cm^{-3})
B1......	1.66	2.29	1.08
B2......	4.78	7.96	3.76

From the Doyle & Keenan paper (1992, their Table 2) we calculate the value of $Ne^2\delta h$, where δh is the height over which the Si IV line is emitting. We find the emission measure per unit area SEM (Table 2) assuming a pressure of 30 dyne cm^{-2}.

Then if we take as the area of the bright point one pixel of $3'' \times 3''$, we obtain the emission measure, EM, given in Table 2. Using the spectrum where the Si IV λ1402.8 and the O IV λ1401.2 lines lie, we derive the electron density from the intensity ratio of these two lines (Feldman & Doschek 1978). We measure an intensity ratio of 8.2 for the lines in the region under study and derive an electron density of 10^{11} cm^{-3}. A lower pressure in the previous computation does not change the result significantly.

If we compare these values with those of Table 1, we notice a difference of 2 orders of magnitude between the emission measures of the X-rays and the UV lines. This emission may actually be from different plasmas, with the X-ray–emitting plasma from a region somewhat above the transition region. Conservation of pressure leads to a transition region thinner by a factor 10^{-2} compared to the hot plasma. Another possibility is that the X-rays are coming from the core of a structure that is heated, for example, by deposition of nonthermal particle energy. This emission is therefore very transient in nature, as it will persist for only as long as the intense energy deposition is present; a less intense energy deposition will power the UV-emitting plasma without ever producing the conditions for thermal X-ray emission. Both before and after the X-ray burst the majority of the energy serves to heat the bulk of the structure. Thus the emission measure for the lower temperature emission is significantly higher than for the transient X-ray–emitting plasma. The X-rays might also be nonthermal, and then a mechanism such as that discussed by Simnett & Haines (1990) easily accounts for the differences in emission between X-rays and UV; however, in this case the interpretation of the X-rays using the HXIS Counting Rate Prediction Programme is invalid, as this programme specifically addresses thermal emission.

Yet another possibility may be that unresolved loops at different temperatures are contributing to the overall emission.

4. CONCLUSION

In the active region AR 2725 on October 13 we have observed two different regions according to their magnetic configurations. In the strong-shear region we observe subflares and a twisted filament. In the low-shear region we observe an arch filament system and UV bright loops in a nearly potential configuration due to continuous emergence of new flux. The hard X-ray emission of this latter region is enhanced at the time of the subflares, with some slight delay suggesting the propagation of an Alfvén wave between the two sites.

UV bright points that we have presented in this paper seem to occur only along the inversion line of the magnetic field. In fact, small emergence of new flux has stronger effects in low field strength regions than in a high field region; in a low magnetic field strength region a small change leads to a complex magnetic field topology and possible reconnection with the ambient coronal field. The energy cannot be stored for long times and only small energy events occur.

Such short-lived bright points were frequently observed in active regions with the UVSP instrument (Porter, Toomre, & Gebbie; Porter et al. 1987; Hayes & Shine 1987) and they were shown to be correlated with small X-ray events (Porter, Fontenia, & Simnett, 1994). Their characteristics are similar to the recent EUV blinkers observed by CDS spectrometer on board *SOHO* (Harrison 1997). The blinkers are observed in the quiet Sun at the network junctions, again along the inversion magnetic field line where a weak emerging flux can have some importance for reconnection and for heating the plasma.

The authors would like to thank Dr. Harvey for providing magnetic data from Kitt Peak National Observatory, Dr. G. Doyle for discussing on the physical parameters derived from Si IV intensity, and the anonymous referee who helps us to clarify some points. The STARLINK facility at the University of Birmingham was used to process the HXIS data. The MSDP data were digitalized by the microdensitometer of Paris (MAMA). This work was achieved in the frame of the French Argentina programme: ECOS A97U01.

REFERENCES

Alissandrakis, C. 1981, A&A, 100, 197
Alissandrakis, C. E., Tisiropoula, G., & Mein, P. 1990, A&A, 230, 200
Amari, T., Luciani, J. F., Aly, J. J., & Mikić, Z. 1997, in Coronal Mass Ejections, ed. N. Crooker, J. A. Joselyn, & J. Feynman, 101
Cheng, C. C., Tandberg-Hanssen, E., Bruner, E. C., Orwig, L., Frost, K. J., Kenny, P. J., Woodgate, B. E., Shine, R. A. 1981, ApJ, 248, L39
Démoulin, P., Bagalá, L. G., Mandrini, C. H., Hénoux, J. C., & Rovira, M. G. 1997, A&A, 325, 305
Doyle, J. D., & Keenan, F. P. 1992, A&A, 264, 173
Feldman, U., & Doschek, G. A. 1978, ApJ, 652, 15
Harrison, R. A. 1997, Sol. Phys., 175, 467
Hayes, M., & Shine, R. A. 1987, ApJ, 312, 943
Klimchuk, S. A. 1987, ApJ, 323, 368
Li Jink, Metcalf, R., Canfield, R. C., Wülster, J.-P., & Kosugi, T. 1997, ApJ, 482, 490
Malherbe, J. M., Schmieder, B., Mein, P., Mein, N., van Driel-Gesztelyi, L., & von Uexküll, M. 1998, Sol. Phys., 180, 265
Mein, P. 1977, Sol. Phys., 54, 45
Mein, P., Démoulin, P., Mein, N., Engvold, O., Molowny-Horas, R., Heinzel, P., & Gontikakis, C. 1996, A&A, 305, 343
Mewe, R. & Gronenschild, E. H. B. M. 1981, A&AS, 45, 11
Porter, J. G., Fontenla, J. M., & Simnett, G. M. 1994, ApJ, 438, 472
Porter, J. G., Moore, R. L., Reichmann, E. J., Engvold, O., & Harvey, K. L. 1987, ApJ, 323, 380
Porter, J. G., Toomre, J., & Gebbie, K. B. 1984, ApJ, 283, 879
Sakao, T., Kosugi, K., Masuda, S., Makishima, K., Inda-Koide, M., & Murakami, T. 1998, PASJ, in press
Schmieder, B., Raadu, M. A., & Wiik, J. E. 1991, A&A, 253, 353
Schmieder, B., Rovira, M., Simnett, G. M., Fontenla, J. M., & Tandberg-Hanssen, E. 1996, A&A, 308, 969
Simnett, G. M. 1983, Sol. Phys., 86, 298
Simnett, G. M., & Haines, M. G. 1990, Sol. Phys., 130, 253
Simnett, G. M., & Strong, K. T. 1996, ApJ, 284, 839
Tandberg-Hanssen, E., Reichmann, E., & Woodgate, B. 1983, Sol. Phys., 86, 159
Teuber, D., Tandberg-Hanssen, E., & Hagyard, M. J. 1977, Sol. Phys., 53, 97
Woodgate, B., et al. 1980, Sol. Phys., 65, 73